



Title	Cellular Interactions and Formation of an Epithelial “Nanocoating-Like Barrier” with Mesoporous Silica Nanoparticles
Author(s)	LI, X; Pang, KY; Ng, TW; Leung, PC; Zhang, C; Leung, KCF; Jin, L
Citation	Nanomaterials, 2016, v. 6, p. 192
Issued Date	2016
URL	http://hdl.handle.net/10722/244794
Rights	This work is licensed under a Creative Commons Attribution-NonCommercial-NoDerivatives 4.0 International License.



Communication

Cellular Interactions and Formation of an Epithelial “Nanocoating-Like Barrier” with Mesoporous Silica Nanoparticles

Xuan Li ¹, Ka Yan Pang ¹, Tsz Wing Ng ², Ping Chung Leung ³, Cheng Fei Zhang ¹, Ken Cham-Fai Leung ^{2,*} and Lijian Jin ^{1,*}

¹ Faculty of Dentistry, The University of Hong Kong, Hong Kong, China; lixuanlwj@hotmail.com (X.L.); nisdabendan@gmail.com (K.Y.P.); zhangcf@hku.hk (C.F.Z.)

² Department of Chemistry, Institute of Creativity, and Partner State Key Laboratory of Environmental & Biological Analysis, The Hong Kong Baptist University, Kowloon, Hong Kong, China; 12018112@life.hkbu.edu.hk

³ Institute of Chinese Medicine and Partner State Key Laboratory of Phytochemistry & Plant Resources in West China, The Chinese University of Hong Kong, New Territories, Hong Kong, China; pingcleung@cuhk.edu.hk

* Correspondence: cfleung@hkbu.edu.hk (K.C.-F.L.); ljjin@hku.hk (L.J.); Tel.: +852-3411-2319 (K.C.-F.L.); +852-2859-0302 (L.J.)

Academic Editor: Thomas Nann

Received: 2 September 2016; Accepted: 19 October 2016; Published: 27 October 2016

Abstract: Oral mucosa as the front-line barrier in the mouth is constantly exposed to a complex microenvironment with multitudinous microbes. In this study, the interactions of mesoporous silica nanoparticles (MSNs) with primary human gingival epithelial cells were analyzed for up to 72 h, and their diffusion capacity in the reconstructed human gingival epithelia (RHGE) and porcine ear skin models was further assessed at 24 h. It was found that the synthesized fluorescent mesoporous silica nanoparticles (RITC-NPs) with low cytotoxicity could be uptaken, degraded, and/or excreted by the human gingival epithelial cells. Moreover, the RITC-NPs penetrated into the stratum corneum of RHGE in a time-dependent manner, while they were unable to get across the barrier of stratum corneum in the porcine ear skins. Consequently, the penetration and accumulation of RITC-NPs at the corneum layers of epithelia could form a “nanocoating-like barrier”. This preliminary proof-of-concept study suggests the feasibility of developing nanoparticle-based antimicrobial and anti-inflammatory agents through topical application for oral healthcare.

Keywords: nanoparticles; human gingival epithelium; coating; stratum corneum

1. Introduction

In recent years, nanotechnology has gained great attention and been increasingly applied to different disciplines in healthcare. The inorganic mesoporous silica nanoparticles (MSNs) have been extensively studied and further developed into various cutting-edge technologies for bio-imaging, cancer therapy, drug delivery, and solid supports of molecular or supramolecular switches owing to their unique features [1–3]. Plenty of in vivo studies have investigated their bio-distribution, accumulation, and clearance in certain tissues via intravenous injection [4–6]. However, there is still no consensus on the bio-safety of nanomaterials [7]. Comparing with intravenous injection, topical application could enhance the safety of nanomaterials by keeping them away from the circulation at a certain level [8]. Thereby, the critical concerns of the accumulation of nanomaterials in the targeting tissues or organs should be addressed carefully. As such, further understanding on

the delicate interactions of these nanoparticles with normal epithelia cells is crucial for assessing the potential risks of their applications in topical medications.

It is well noted that porcine ear skin as a valid *in vitro* model could provide convincing results with human skin in transdermal study due to their structural similarity and comparable biochemical properties [9]. Meanwhile, oral mucosa containing both keratinized and non-keratinized epithelia can be stratified as the epidermis of skin [10]. Gingival epithelia consisting of both keratinized oral epithelia and non-keratinized sulcular epithelia are on the front line of innate host response to microbial challenge, and critically account for periodontal health. Gingival niche is indeed a critical target for the delivery of anti-infective and -inflammatory agents in tackling one of the most common diseases in humans, i.e. the periodontal (gum) disease. Previous studies have compared the differences in the permeability of water and nicotine across oral mucosa and skin [11–13]. However, it remains unclear on the exact diffusion capacity of nanoparticles in the oral mucosa, as well as the potential difference in the penetration of nanomaterials in oral mucosa and skin. Hence, based on our recent work [14], we synthesized the fluorescent mesoporous silica nanoparticles (RITC-NPs), analyzed their interactions with the primary human gingival epithelial cells (hGECs), and subsequently evaluated their penetration efficiency in two representative epithelial structures of the reconstructed human gingival epithelia (RHGE) and porcine ear skin models.

2. Results

The scanning electron microscope (SEM) images showed that the fabricated MSNs and RITC-NPs presented shapes from spheres to ellipsoids (Figure 1a,b). The average size and Zeta potential of RITC-NPs were 271.9 ± 171.2 nm and 18.49 mv, respectively (Figure 1c). Under UV excitation, the RITC-NPs emitted an obvious red fluorescence (Figure S1). Their cytotoxicity was evaluated on the hGECs using Cell Counting Kit-8. Notably, the RITC-NPs exhibited less cytotoxicity on the cells with reference to the bare MSNs at the same concentration (200 $\mu\text{g}/\text{mL}$) (Figure 1d), probably due to the enlarged nanoparticle size after surface modification and fluorescent labeling [15].

Next, the fluorescent images showed that the RITC-NPs could be internalized by the hGECs at 24 h (Figure 2b). After incubation in the nanoparticle-free medium for another 24 and 48 h, small amounts of RITC-NPs remained in the cells (Figure 2c,d). As common fluorescent dyes with stable performance in the acidic and enzymatic environment, rhodamine B and its derivatives have been developed as fluorescent probes for lysosomal labeling and tracking [16]. Notably, it has been confirmed that silica nanoparticles can be degraded intracellularly [17] and released by cells [18], which could account for the observation of the decrease of fluorescence intensity in the cells (Figure 2c,d and Figure 3). Our observations were consistent with previous findings on the internalization and expulsion of MSNs in mammal cells [18–20]. However, most of these studies were conducted on cancer cell lines or phagocytic cells, and they varied greatly in cellular activities and functions with normal primary cells [21]. Taken together, our current findings suggest that the fabricated MSNs with low cytotoxicity could be internalized and intracellularly degraded and/or released by the primary human gingival epithelial cells. Further study is required to clarify this point. The epithelial penetration efficiency of RITC-NPs was examined on two representative epithelial structures, i.e., isolated porcine ear skin and RHGE that have a histological structure similar to human gingiva (Figure S2a) [22]. Interestingly, the RITC-NPs penetrated into the stratum corneum of RHGE in a time-dependent manner (Figure 4a–h). After 2 h treatment, only light red fluorescence dots and lines were visualized on the top of stratum corneum layer in the RHGE (Figure 4c,d), and the fluorescence intensity increased at 6 h (Figure 4e,f) and markedly enhanced at 24 h (Figure 4g,h). Surprisingly, no fluorescent signal was detected at the deeper layers of RHGE after 24 h treatment, suggesting the penetration and accumulation of RITC-NPs within the corneum layer of RHGE. However, the penetration profile of RITC-NPs was to some extent different in the porcine ear skin model. The fluorescent light was visible at 2 h, and it became more obvious at 6 h (Figure 4k–n). However, no obvious fluorescence nanoparticles were detected beyond the stratum corneum even after 24 h treatment, as it could act as a natural epithelial barrier and repel the RITC-NPs (Figure 4o,p). In addition, the hair follicles in the porcine ear skin provided other routes

for the accumulation of RITC-NPs, whereas they were not able to critically go across the follicular barrier into the underlying dermis (Figure S3). This finding supports the notion that hair follicles could be a potential target of the nanomaterials-based drug delivery vehicles [23]. Overall, a fairly even penetration and distribution of nanoparticles in the corneum layer were observed in the two selected epithelial structures, following 24 h treatment of RITC-NPs in the RHGE and porcine ear skin.

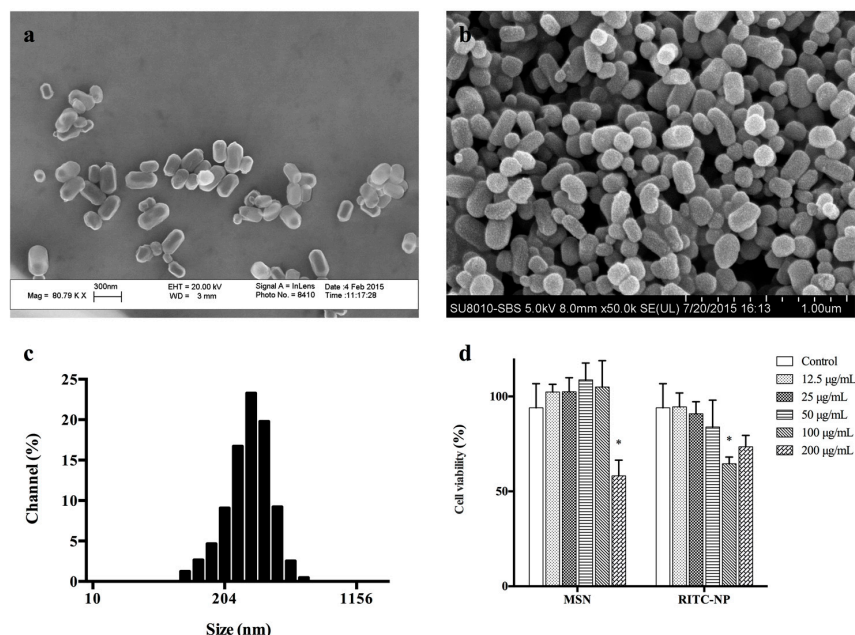


Figure 1. Field emission scanning electron microscope (FE-SEM) images of the mesoporous silica nanoparticles (MSNs) (a) and synthesized fluorescent mesoporous silica nanoparticles (RITC-NPs) (b), and the size distribution of RITC-NPs analyzed by dynamic light scattering (DLS) (c). The viability of human gingival epithelial cells (hGECs) after 24 h treatment with various concentrations of MSNs and RITC-NPs was assessed using the Cell Counting Kit-8 (CCK-8) by measuring the absorbance (450 nm) of the supernatant (d). Three independent experiments were undertaken in triplicate. The asterisk (*) indicates the significant difference ($p < 0.05$) between the control and treatment groups.

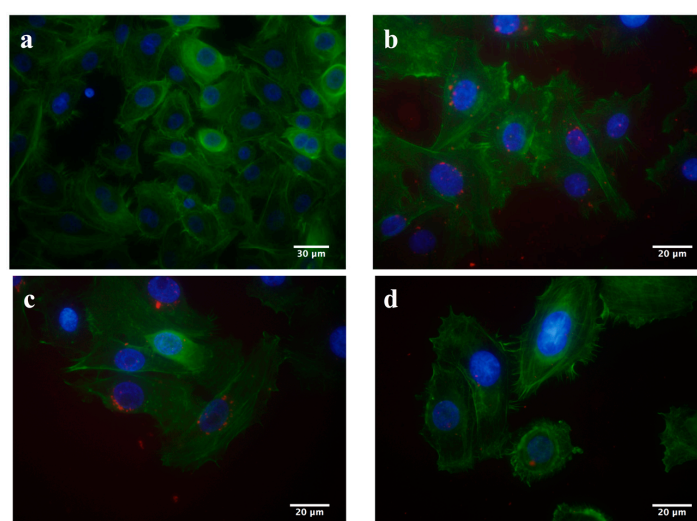


Figure 2. Fluorescent images of the hGECs incubated with the RITC-NPs for 0 h as the control (a) and 24 h (b). The cells were further incubated in the nanoparticle-free medium for another 24 h (c) and 48 h (d). The cell nuclei and cytoskeletal F-actin fibers were fluorescently stained with blue and green, respectively. The red fluorescence represents RITC-NPs.

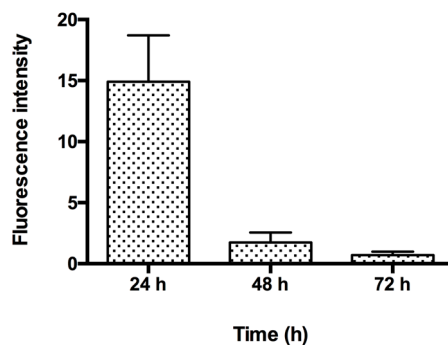


Figure 3. The fluorescence intensity of RITC-NPs in hGECs after co-incubation for 24 h, followed by another 24 and 48 h incubation in the nanoparticle-free media. Error bars represent the standard deviation of three replicates.

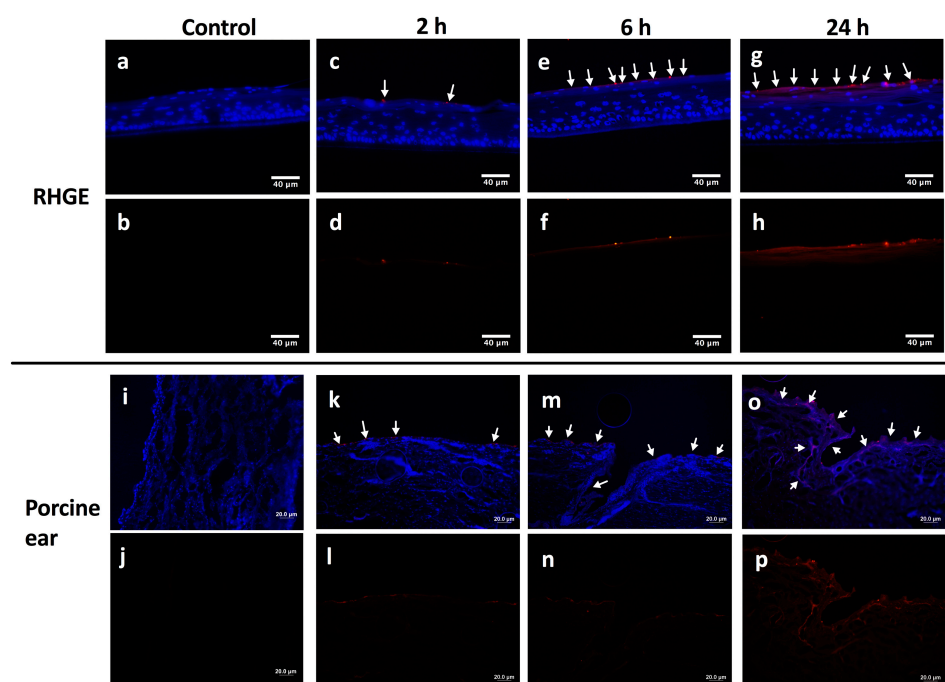


Figure 4. The merged fluorescent images and red fluorescent channels of RITC-NPs in the reconstructed human gingival epithelia (RHGE) at 0 (a,b), 2 (c,d), 6 (e,f) and 24 h (g,h) as well as the porcine ear skin at 0 (i,j), 2 (k,l), 6 (m,n) and 24 h (o,p). The blue and red fluorescence reflects the cell nuclei and RITC-NPs, respectively. Scale bars: 40 μm in RHGE images and 20 μm in porcine ear skin images.

3. Discussion

Porcine ear skin as a well-established *in vitro* model has been frequently used to test the penetration capacity of different nanomaterials, such as carbon nanotubes, quantum dots, and polystyrene nanoparticles [24,25]. Although silica nanoparticles have been investigated in different cell models, there are a limited number of studies on their penetration and permeation through skins. Generally, silica nanoparticles with an average size less than 25 nm can penetrate but could not permeate the skin [24]. As the vehicles of quercetin, MSNs with an average size of 250 nm can facilitate drug penetration in the skin while without transdermal delivery [26]. This could be due to the barrier property of stratum corneum. Moreover, the silica nanoparticles with a diameter of 42 nm were found to be present around the epidermal cells through topical allocation, owing to partial disruption of the stratum corneum of human skin explants [27]. Our findings enhance the possible role of barrier property of stratum corneum in response to the nanoparticle penetration.

Oral mucosa as the front-line barrier is constantly exposed to a complex and dynamic microenvironment with multitudinous microbes. Periodontal disease is one of the most common oral diseases and major health burdens globally, and it results from dental plaque biofilms-induced, dysregulated immuno-inflammatory response [28,29]. Human gingiva is “armed” by a cluster of innate defense molecules through dynamic interactions with microbes [30]. Therefore, effective control of plaque biofilms and gingival inflammation is crucial for periodontal health [31]. In the present study, it was found that MSNs with low cytotoxicity could penetrate while accumulate predominantly in the stratum corneum of the RHGE after 24 h treatment. As such, a form of “nanocoating-like barrier” could be generated along the superficial layers of the epithelia. It is noted that the human gingival epithelia constantly maintain self-renewal via detaching aged corneum layers and the regulated movement of keratinized gingival epithelial cells toward the superficial layers [10].

4. Materials and Methods

4.1. Reagents

The chemicals including cetyltrimethylammonium bromide (CTAB), 3-aminopropyltriethoxy silane (APTES), and rhodamine B isothiocyanate (RITC) were obtained from Sigma-Aldrich (St. Louis, MO, USA), and tetraethyl orthosilicate (TEOS) as the silica source was purchased from Acros Organics (Thermo Fisher Scientific, Waltham, MA, USA). Aqueous ammonia and 37% hydrochloric acid were ordered from VWR (Radnor, PA, USA) and RCI Labscan (Bangkok, Thailand), respectively.

4.2. Fabrication and Characterization of Fluorescence-Labeled MSNs

The nanoparticles were synthesized and surface-modified according to our recent report [14]. Briefly, 0.36 g of CTAB were dissolved in 180 mL of distilled water at 30 °C to obtain the clear solution. An amount of 5 mL of aqueous ammonia was subsequently added into the solution as a catalyst. TEOS (1.56 mL) was suspended in 10 mL of ethanol, and the suspension was then dropped into the solution at 1 mL/min and stirred for 5 h at room temperature. After 24 h, the MSNs were collected following centrifugation (6000 rpm for 10 min) using a centrifuge (5804, Eppendorf, Hamburg, Germany). The surfactant was removed by sonication twice in acidic ethanol for further usage. To graft the amine functional groups on the MSNs, 0.5 g of MSNs were dispersed in 100 mL of ethanol and refluxed with 1.25 mL APTES overnight. The amine-modified MSNs (APTES-NPs) were subsequently harvested by centrifugation. After being washed with ethanol twice, 0.2 g of the oven-dried APTES-NPs were dispersed in a sealed RITC ethanol solution (0.125 mg/mL, 40 mL) with magnetic stirring for 4 h at room temperature. The fluorescence-labeled MSNs were collected by centrifugation followed by ethanol washing twice. The MSNs and RITC-NPs were properly dried in vacuum, and the morphology was analyzed via LEO1530 field emission scanning microscopy (FE-SEM, Zeiss, Oberkochen, Germany) and SU8010 FE-SEM (Hitachi, Tokyo, Japan), respectively. The average size and Zeta potential of the RITC-NPs were analyzed by Nanotracer Wave (Microtrac, San Diego, CA, USA). The fluorescence of RITC-NPs was excited using UV light and visualized by naked eyes.

4.3. Cell Culture and Viability Assay

The hGECs were purchased from CellnTec Advanced Cell Systems AG (Bern, Switzerland), and cultured in a CnT-24 medium with supplements (CellnTec) and 1% penicillin. The cells were cultured at 37 °C with 5% CO₂ in the humidified incubator. After reaching the confluence, the 3rd passage of hGECs was seeded in a 96-well plate at a density of 2×10^4 cells/well and subsequently treated with the MSNs or RITC-NPs at various concentrations (200, 100, 50, 25, and 12.5 µg/mL) for 24 h. The cell viabilities were assessed by the Cell Counting Kit-8 (Sigma-Aldrich, St. Louis, MO, USA). In brief, 100 µL of the medium in each well were discarded, and 10 µL of CCK-8 solution were then added and incubated for 2 h. The absorbance of the media was measured at 450 nm by a microplate reader (SpectraMax M2, Molecular Devices, Sunnyvale, CA, USA).

4.4. The Internalizations of RITC-NPs with hGECs

The hGECs at 4th passage (2×10^4 cells/well) were cultured in 16-well glass slides (Nunc™ Lab-Tek™ II Chamber Slide™ System, Thermo Scientific, Waltham, MA, USA), and treated with 50 µg/mL of RITC-NPs for 24 h. Then, the medium was removed, and the cells were washed gently with phosphate buffered saline (PBS) twice. The cells were subsequently fixed with 3.7% formaldehyde for 10 min at room temperature and then stained with Alexa Fluor® 488 Phalloidin. After the staining, the cells were washed again with the PBS. The gasket of the slide was removed, and the cells were mounted with a Fluoro-Gel II mounting medium containing DAPI (Electron Microscopy Sciences, Hatfield, PA, USA) and covered by the coverslips. The interaction of RITC-NPs with the cells were visualized by an Olympus 1 × 2-UCB fluorescent microscope (Tokyo, Japan). The fluorescence intensity of RITC-NPs in the cells was examined according to the methods described by Harush-Frenkel and co-workers with some modifications [32]. In order to assess the amount of the RITC-NPs in the hGECs, the cells were seeded at a density of 2×10^4 cells/well in 96-well plates and treated with the RITC-NPs (50 µg/mL) for 24 h. The media were removed, and the cells were washed gently with the PBS twice. A fresh blank medium was added to the cells and changed every 24 h. At each time point, the fluorescence intensity of the RITC-NPs in the cells was determined by the Microplate Reader (SpectraMax M2, Molecular Devices, Sunnyvale, CA, USA) with excitation and emission wavelengths of 543 and 580 nm, respectively.

4.5. Preparation and Characterization of the Porcine Ear Skin and Reconstructed Human Gingival Epithelia

Porcine ears were obtained from a local market after the pigs were freshly sacrificed. The ear skin was carefully removed from the underlying cartilage using a scalpel and was then incubated in Dulbecco's PBS (Thermo Fisher, Waltham, MA, USA) at 37 °C for the permeability experiment. The reconstructed human gingival epithelia (RHGE) were purchased from the Episkin (Nice, France) and cultured in the SkinEthic maintenance medium (Episkin, Nice, France) on inert polycarbonate filters (0.5 cm²) at 37 °C in a humidified incubator with 5% CO₂. Both porcine ear skin and RHGE were processed in formalin, dehydrated, and embedded in paraffin for histological staining.

4.6. Penetration Tests of the RITC-NPs

An area of the porcine ear skin was cut out using surgical scissors according to the shape and size of the contact point on the Franz diffusion cells (17 mL, Red & Blue Medicine Technical Equipment, Nanjing, China). It was then placed in a sandwiched way such that the epithelial portion faced the donor compartment and the underlying connective tissues toward the receiver compartment. The dispersion of RITC-NPs (200 µg/mL) was prepared via sonication in PBS for 10 min and then added to the donor compartment. The incubation was carried out at 37 °C using the Automatic Transdermal Apparatus (TP-6, Red & Blue Medicine Technical Equipment, Nanjing, China). The tissues were harvested at 0, 2, 6, and 24 h, and the surfaces were washed with PBS twice to remove the loosely adhered RITC-NP. Subsequently, the tissues were fixed in 4% paraformaldehyde and dehydrated in a gradient sucrose solution (10%, 20% and 30%). They were embedded in a Tissue-Tek O.C.T. compound (Sakura Finetek, VWR, Radnor, PA, USA) for cryosection. On arrival, the RHGE were immediately removed from the agarose gel and placed carefully onto 6-well plates containing 1 mL of a maintenance medium for incubation overnight. Well-dispersed RITC-NPs at 200 µg/mL were added to the RHGE topically. They were incubated for 0, 2, 6, and 24 h and then harvested with PBS washing. The samples were fixed in 4% paraformaldehyde, dehydrated, and embedded in an O.C.T. compound for cryosection. All cryosections were mounted with a Fluoro-Gel II mounting medium containing DAPI (Electron Microscopy Sciences, Hatfield, PA, USA) and observed under an Olympus 1 × 2-UCB fluorescent microscope (Tokyo, Japan).

4.7. Statistical Analysis

The significant difference between the testing and control groups was analyzed by a one-way ANOVA using GraphPad Prism 6.

5. Conclusions

The present findings show the observable profiles of the interactions of fluorescent silica nanoparticles with primary gingival epithelial cells, and their notable penetration and accumulation at the superficial corneum layers of epithelia. This preliminary proof-of-concept study strongly suggests the feasibility of developing MSN-based anti-infective and anti-inflammatory agents in topical applications for effective oral healthcare.

Supplementary Materials: The following are available online at www.mdpi.com/2079-4991/6/11/192/s1.

Acknowledgments: This work was supported by the General Research Fund (GRF) from the Hong Kong Research Grants Council (HKU767512 to Lijian Jin and HKBU201213 to Ken Cham-Fai Leung) and the Modern Dental Laboratory/HKU Endowment Fund to Lijian Jin. We thank Xinmiao Lan from The University of Hong Kong, Elaine Wat, and Clara Bik San Lau from The Chinese University of Hong Kong for their technical support.

Author Contributions: Xuan Li, Ken Cham-Fai Leung, and Lijian Jin conceived and designed the experiments; Xuan Li, Ka Yan Pang and Tsz Wing Ng performed the experiments; Xuan Li, Ping Chung Leung, Cheng Fei Zhang, Ken Cham-Fai Leung and Lijian Jin analyzed the data; Ping Chung Leung, Ken Cham-Fai Leung and Lijian Jin contributed reagents/materials/analysis tools; Xuan Li, Ken Cham-Fai Leung and Lijian Jin wrote the paper.

Conflicts of Interest: The authors declare no conflict of interest.

Abbreviations

The following abbreviations are used in this manuscript:

MSNs	mesoporous silica nanoparticles
hGECs	human gingival epithelial cells
RHGE	reconstructed human gingival epithelia
RITC-NPs	fluorescent mesoporous silica nanoparticles
DLS	dynamic light scattering
CTAB	cetyltrimethylammonium bromide
APTES	3-aminopropyltriethoxy silane
RITC	rhodamine B isothiocyanate
TEOS	tetraethyl orthosilicate
FE-SEM	field emission scanning electron microscope
PBS	phosphate buffered saline

References

- Lim, W.Q.; Phua, S.Z.F.; Xu, H.V.; Sreejith, S.; Zhao, Y. Recent advances in multifunctional silica-based hybrid nanocarriers for bioimaging and cancer therapy. *Nanoscale* **2016**, *8*, 12510–12519. [[CrossRef](#)] [[PubMed](#)]
- Song, N.; Yang, Y.-W. Molecular and supramolecular switches on mesoporous silica nanoparticles. *Chem. Soc. Rev.* **2015**, *44*, 3474–3504. [[CrossRef](#)] [[PubMed](#)]
- Mamaeva, V.; Sahlgren, C.; Lindén, M. Mesoporous silica nanoparticles in medicine-recent advances. *Adv. Drug Deliv. Rev.* **2013**, *65*, 689–702. [[CrossRef](#)] [[PubMed](#)]
- Cho, M.; Cho, W.S.; Choi, M.; Kim, S.J.; Han, B.S.; Kim, S.H.; Kim, H.O.; Sheen, Y.Y.; Jeong, J. The impact of size on tissue distribution and elimination by single intravenous injection of silica nanoparticles. *Toxicol. Lett.* **2009**, *189*, 177–183. [[CrossRef](#)] [[PubMed](#)]
- Huang, X.; Li, L.; Liu, T.; Hao, N.; Liu, H.; Chen, D.; Tang, F. The shape effect of mesoporous silica nanoparticles on biodistribution, clearance, and biocompatibility in vivo. *ACS Nano* **2011**, *5*, 5390–5399. [[CrossRef](#)] [[PubMed](#)]
- Liu, T.; Li, L.; Teng, X.; Huang, X.; Liu, H.; Chen, D.; Ren, J.; He, J.; Tang, F. Single and repeated dose toxicity of mesoporous hollow silica nanoparticles in intravenously exposed mice. *Biomaterials* **2011**, *32*, 1657–1668. [[CrossRef](#)] [[PubMed](#)]
- Valsami-Jones, E.; Lynch, I. How safe are nanomaterials? *Science* **2015**, *350*, 388–389. [[CrossRef](#)] [[PubMed](#)]

8. Ryu, H.J.; Seong, N.W.; So, B.J.; Seo, H.S.; Kim, J.H.; Hong, J.S.; Park, M.K.; Kim, M.S.; Kim, Y.R.; Cho, K.B.; et al. Evaluation of silica nanoparticle toxicity after topical exposure for 90 days. *Int. J. Nanomed.* **2014**, *9*, 127–136.
9. Godin, B.; Touitou, E. Transdermal skin delivery: Predictions for humans from in vivo, ex vivo and animal models. *Adv. Drug Deliv. Rev.* **2007**, *59*, 1152–1161. [[CrossRef](#)] [[PubMed](#)]
10. Jones, K.B.; Klein, O.D. Oral epithelial stem cells in tissue maintenance and disease: The first steps in a long journey. *Int. J. Oral Sci.* **2013**, *5*, 121–129. [[CrossRef](#)] [[PubMed](#)]
11. Lesch, C.; Squier, C.; Cruchley, A.; Williams, D.; Speight, P. The permeability of human oral mucosa and skin to water. *J. Dent. Res.* **1989**, *68*, 1345–1349. [[CrossRef](#)] [[PubMed](#)]
12. Nair, M.K.; Chetty, D.J.; Ho, H.; Chien, Y.W. Biomembrane permeation of nicotine: Mechanistic studies with porcine mucosae and skin. *J. Pharm. Sci.* **1997**, *86*, 257–262. [[CrossRef](#)] [[PubMed](#)]
13. Squier, C.A.; Cox, P.; Wertz, P.W. Lipid content and water permeability of skin and oral mucosa. *J. Investig. Dermatol.* **1991**, *96*, 123–126. [[CrossRef](#)] [[PubMed](#)]
14. Li, X.; Wong, C.-H.; Ng, T.-W.; Zhang, C.-F.; Leung, K.C.-F.; Jin, L. The spherical nanoparticle-encapsulated chlorhexidine enhances anti-biofilm efficiency through an effective releasing mode and close microbial interactions. *Int. J. Nanomed.* **2016**, *11*, 2471–2480.
15. Napierska, D.; Thomassen, L.C.; Rabolli, V.; Lison, D.; Gonzalez, L.; Kirsch-Volders, M.; Martens, J.A.; Hoet, P.H. Size-dependent cytotoxicity of monodisperse silica nanoparticles in human endothelial cells. *Small* **2009**, *5*, 846–853. [[CrossRef](#)] [[PubMed](#)]
16. Yapici, N.B.; Bi, Y.; Li, P.; Chen, X.; Yan, X.; Mandalapu, S.R.; Faucett, M.; Jockusch, S.; Ju, J.; Gibson, K.M.; et al. Highly stable and sensitive fluorescent probes (lysoprobes) for lysosomal labeling and tracking. *Sci. Rep.* **2015**, *5*, 8576. [[CrossRef](#)] [[PubMed](#)]
17. Kempen, P.J.; Greasley, S.; Paker, K.A.; Campbell, J.L.; Chang, H.Y.; Jones, J.R.; Sinclair, R.; Gambhir, S.S.; Jokerst, J.V. Theranostic mesoporous silica nanoparticles biodegrade after pro-survival drug delivery and ultrasound/magnetic resonance imaging of stem cells. *Theranostics* **2015**, *5*, 631–642. [[CrossRef](#)] [[PubMed](#)]
18. Chu, Z.; Huang, Y.; Tao, Q.; Li, Q. Cellular uptake, evolution, and excretion of silica nanoparticles in human cells. *Nanoscale* **2011**, *3*, 3291–3299. [[CrossRef](#)] [[PubMed](#)]
19. He, Q.; Zhang, Z.; Gao, Y.; Shi, J.; Li, Y. Intracellular localization and cytotoxicity of spherical mesoporous silica nano- and microparticles. *Small* **2009**, *5*, 2722–2729. [[CrossRef](#)] [[PubMed](#)]
20. Slowing, I.; Trewyn, B.G.; Lin, V.S. Effect of surface functionalization of MCM-41-type mesoporous silica nanoparticles on the endocytosis by human cancer cells. *J. Am. Chem. Soc.* **2006**, *128*, 14792–14793. [[CrossRef](#)] [[PubMed](#)]
21. Oh, N.; Park, J.-H. Endocytosis and exocytosis of nanoparticles in mammalian cells. *Int. J. Nanomed.* **2014**, *9*, 51–63.
22. Wurzburger, L.; Kazmi, P.; Re, T.; Alonso, A.; Bertino, B.; Barnes, N.; de Brugerolle de Fraissinette, A.; Hilberer, A.; Raabe, H.; Wilt, N.; et al. Evaluation of an oral care product safety screening program utilizing the in vitro skinethic human gingival epithelium (RHG) and oral buccal (RHO) models. In Proceedings of the 50th SOT Annual Meeting, Washington, DC, USA, 6–10 March 2011.
23. Lademann, J.; Knorr, F.; Richter, H.; Jung, S.; Meinke, M.; Rühl, E.; Alexiev, U.; Calderón, M.; Patzelt, A. Hair follicles as a target structure for nanoparticles. *J. Innov. Opt. Health Sci.* **2015**, *8*, 1530004. [[CrossRef](#)]
24. Filon, F.L.; Mauro, M.; Adami, G.; Bovenzi, M.; Crosera, M. Nanoparticles skin absorption: New aspects for a safety profile evaluation. *Regul. Toxicol. Pharmacol.* **2015**, *72*, 310–322. [[CrossRef](#)] [[PubMed](#)]
25. Schneider, M.; Stracke, F.; Hansen, S.; Schaefer, U.F. Nanoparticles and their interactions with the dermal barrier. *Derm. Endocrinol.* **2009**, *1*, 197–206. [[CrossRef](#)]
26. Sapino, S.; Ugazio, E.; Gastaldi, L.; Mileto, I.; Berlier, G.; Zonari, D.; Oliaro-Bosso, S. Mesoporous silica as topical nanocarriers for quercetin: Characterization and in vitro studies. *Eur. J. Pharm. Biopharm.* **2015**, *89*, 116–125. [[CrossRef](#)] [[PubMed](#)]
27. Rancan, F.; Gao, Q.; Graf, C.; Troppens, S.; Hadam, S.; Hackbarth, S.; Kembuan, C.; Blume-Peytavi, U.; Rühl, E.; Lademann, J. Skin penetration and cellular uptake of amorphous silica nanoparticles with variable size, surface functionalization, and colloidal stability. *ACS Nano* **2012**, *6*, 6829–6842. [[CrossRef](#)] [[PubMed](#)]
28. Jin, L.J.; Lamster, I.B.; Greenspan, J.S.; Pitts, N.B.; Scully, C.; Warnakulasuriya, S. Global burden of oral diseases: Emerging concepts, management and interplay with systemic health. *Oral Dis.* **2016**, *22*, 609–619. [[CrossRef](#)] [[PubMed](#)]

29. Page, R.C.; Kornman, K.S. The pathogenesis of human periodontitis: An introduction. *Periodontology* **1997**, *14*, 9–11. [[CrossRef](#)]
30. Jin, L.J. An update on innate defense molecules of human gingiva. *Periodontology* **2011**, *56*, 125–142. [[CrossRef](#)] [[PubMed](#)]
31. Bartold, P.M.; Van Dyke, T.E. Periodontitis: A host-mediated disruption of microbial homeostasis. Unlearning learned concepts. *Periodontology* **2013**, *62*, 203–217. [[CrossRef](#)] [[PubMed](#)]
32. Harush-Frenkel, O.; Rozentur, E.; Benita, S.; Altschuler, Y. Surface charge of nanoparticles determines their endocytic and transcytotic pathway in polarized mdck cells. *Biomacromolecules* **2008**, *9*, 435–443. [[CrossRef](#)] [[PubMed](#)]



© 2016 by the authors; licensee MDPI, Basel, Switzerland. This article is an open access article distributed under the terms and conditions of the Creative Commons Attribution (CC-BY) license (<http://creativecommons.org/licenses/by/4.0/>).